AIAA SciTech Forum
11–15 & 19–21 January 2021, VIRTUAL EVENT
AIAA Scitech 2021 Forum

10.2514/6.2021-0196



# Some Considerations Involving Testing Guidelines for Large Curvature Bending of High Strain Composites using the Column Bending Test

Ajay Harihara Sharma *
*University of Colorado, Boulder, Colorado, 80309, USA*

Riley Perez †
*University of Colorado, Boulder, Colorado, 80309, USA*

Nicholas Bearns ‡
*Roccor, LLC, Longmont, CO 80503*
*University of Colorado, Boulder, Colorado, 80309, USA*

TJ Rose §
*Roccor, LLC, Longmont, CO 80503*
*University of Colorado, Boulder, Colorado, 80309, USA*

Francisco López Jiménez¶
*University of Colorado, Boulder, Colorado, 80309, USA*



**The bending properties of High Strain Composites (HSCs) are primarily calculated using the Column Bending Test (CBT). In this paper, we evaluate the effect of variation in certain key parameters involved in CBT: free length of the sample, and the horizontal offset used to trigger bending in a given direction. The results indicate that percentage error in curvature is nearly constant for a given percent error in free length and approximately equal to this percent error in free length value, regardless of the free length value. Regarding the offset, the results indicate that it is desirable to have specimens fail at a higher rotated angle of the rigid arms in order to minimize errors due to an incorrect initial offset distance. We have also explored the effect of subjecting samples to an initial predetermined strain before testing to failure. We found that that pre-conditioning has no effect on the failure strain of samples subjected to bending in order to obtain the moment-curvature response in CBT. Finally, a correction factor has been provided to improve the accuracy of the closed form solution utilized for CBT. This correction factor helps mitigate the error incurred due to the constant curvature assumption in the case when the rigid arms are not sufficiently long compared to the free length of the specimen.**

## I. Introduction

High Strain Composites (HSCs) refer to a class of fiber composite materials that are designed to operate at strains greater than 1% in bending. Structures made of these materials achieve a stowed configuration through mechanisms that rely on the folding of these materials at large curvatures. HSCs are thin laminates consisting of a plastic matrix that is reinforced with carbon or glass fiber. They are of interest for space based applications due to their high stiffness, capacity to withstand large strains, low weight, and their autonomous deployment capabilities (i.e. utilizing strain energy

*Graduate Student, Ann and H.J. Smead Department of Aerospace Engineering Sciences, University of Colorado, Boulder, AIAA Student Member

†Graduate Student, Ann and H.J. Smead Department of Aerospace Engineering Sciences, University of Colorado, Boulder

‡Test and Analysis Intern, Roccor, LLC, Longmont, CO 80503 ; Graduate Student, Ann and H.J. Smead Department of Aerospace Engineering Sciences, University of Colorado, Boulder

§Sr. Mechanical Engineer, Roccor, LLC, Longmont, CO 80503 ; Graduate Student, Ann and H.J. Smead Department of Aerospace Engineering Sciences, University of Colorado, Boulder, AIAA Member.

¶Assistant Professor, Ann and H.J. Smead Department of Aerospace Engineering Sciences, University of Colorado, Boulder, AIAA Member.

as the primary mechanism for deployment rather than relying on external mechanical parts). Examples of structures that utilize HSCs include continuous longeron masts [1], antenna booms [2], spring-back reflector [3], large deployable antennas [4], tape-spring truss [5] and deployable solar arrays [6].

Since HSCs rely on bending as the primary deformation mode, measurement of their bending response is an integral requirement for several deployable structures. However, due to their thinness as well as non-linearity in both geometry as well as material properties, evaluation of their bending response is much more difficult compared to their thicker counterparts. In particular, the bending response of thicker composites is evaluated using the three-point or the four-point bending test. However, those testing methods are only valid for a geometrically linear bending response and cannot characterize large deformations. Several attempts have been made to address this issue.

Pioneering efforts in the field began with the platen test, which was first utilized by Yee and Pellegrino [7] to determine the bending response of thin carbon fiber reinforced composite laminates. However, they observed a highly non-uniform moment distribution throughout the specimen, which made it harder to model moment-curvature. Alternatively, the Large Deformation Four Point Bending Test (LDFPB) was developed to characterize the large curvature bending response of thin CFRP laminates [8]. One disadvantage of this method was that it involved utilization of complicated equipment which made widespread testing of HSCs across different testing groups difficult to pursue. In addition, the coupons tested using LDFPB failed prematurely due to a sudden transition of the stress state at the grips, which lead to concentrated stresses therein. This lead to the development of the Column Bending Test (CBT), which is the currently preferred method for measuring the bending response of thin composite laminates subjected to large curvatures.

CBT was able to overcome the above-mentioned shortcomings of the platen test and LDFPB. The loading obtained from the extension head of the testing machine is converted into rotation of as set of pinned joints. This aids the rotation of a set of rigid arms, which apply a nearly pure moment on the test specimen. The failure of the coupon typically occurs at the center of the specimen, where the maximum moment and curvature occur. If the rigid arms are long enough, the difference between the maximum and the minimum moment is relatively small, and therefore, a constant moment can be assumed throughout the length of the specimen. In order to ensure that the specimen bends in the desired direction at the beginning of the test, the rigid arms are provided with an initial offset distance. A typical CBT setup is shown in Figure 1. Several studies have recently been conducted using CBT to further understand and characterize the test process [9–20].

The objective of the present study is to provide a few recommendations for testing of HSCs using the Column Bending Test. In particular, the topics that would be further explored include:

- Errors in estimated failure curvature due to uncertainty in variation of specimen free length.
- Errors in estimated failure curvature due to incorrect initial offset distance.
- Effect of pre-conditioning (loading and unloading) before testing to failure on estimated failure strain of HSCs.
- Correction factor to improve the accuracy of the closed form solution used for the Column Bending Test.

## II. Analysis of the Column Bending Test using a simplified geometric analysis

The main objective of Column Bending Test is to determine the bending response of HSCs in the geometrically nonlinear regime. For a particular choice of layup, the primary variables of interest obtained from CBT are the failure curvature as well as the slope of the moment versus curvature curve, also known as the bending stiffness ($D_{11}$). It has been shown previously [12] that the bending stiffness of thin CFRP laminates varies as a function of the applied curvature, which is due to the inherent material nonlinearities in carbon fibers. The goal of this section is to review the closed form solution obtained using a simplified geometric analysis of the test.

The primary assumption used to obtain the closed form solution for the Column Bending Test states that the moment and the curvature are constant across the arclength of the bent specimen. Furthermore, since the compressive loading on the specimen is very small, it is also assumed that the length of the specimen does not change during the test. With the help of these two assumptions, it becomes much easier to provide an analytical solution for the maximum curvature and bending moment. The detailed derivation to obtain closed form solution using geometric analysis has been previously discussed [9, 21] and here we present a summary of the main equations used in the closed form solution.

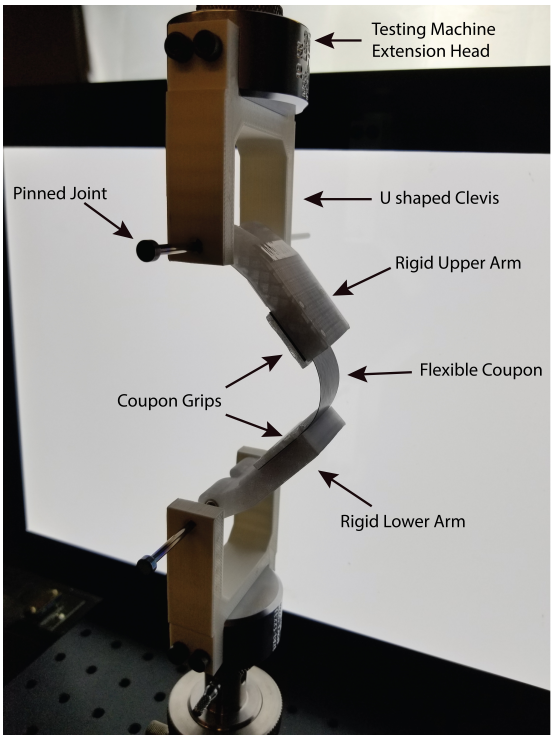


**Fig. 1 Image of the experimental setup used in the Column Bending Test [21].**

Figure 2 shows the geometry of the Column Bending Test [21]. In the equations that follow, $l_s$ represents the gauge length of the sample, assumed to start from the location where the specimen leaves the rigid arms; $l$ represents the effective length of the rigid fixture arm, and represents the distance between the center of the pinned joint, and the point where the specimen leaves the arms; $\theta$ represents the initial angle of the fixture arm obtained due to the initial offset distance; $\phi$ represents the rotation of the fixtures due to the applied loading and the specimen deflection; $\delta$ represents the linear vertical displacement applied by the testing machine; $P$ represents the load applied by the testing machine to the setup; $r$ represents the effective moment arm length between the point of application of the load, and the center of the bent specimen; $a$ represents the linear horizontal distance between the center and the end of the coupon; and $R$ represents the radius of curvature of the bent coupon, assuming it to be a circle.

Applying conservation of vertical distance yields:

$$\frac{\delta}{l_s} = 1 - \frac{2}{\phi}\sin\frac{\phi}{2} + 2\frac{l}{l_s}\left(\cos\theta - \cos\left(\theta + \frac{\phi}{2}\right)\right). \tag{1}$$

Equation 1 needs to be resolved numerically in order to solve for the net rotated angle $\phi$. The curvature is then obtained as $\kappa = \frac{1}{R}$, and using the formula for arclength of a circle, $l_s = R\phi$, yields the formula:

$$\kappa = \frac{\phi}{l_s}. \tag{2}$$

The effective moment armlength $r$ is obtained by equating the distances represented by various variables in the horizontal direction. Upon doing so, the distance $r$ is obtained using:

$$\frac{r}{l_s} = \frac{1}{\phi}\left(1 - \cos\frac{\phi}{2}\right) + \frac{l}{l_s}\sin\left(\theta + \frac{\phi}{2}\right). \tag{3}$$

Using the curvature and the measured value of the thickness, the strain can then be solved for. In reality, due to material non-linearities, the neutral axis does not remain at the center, especially for large curvatures, and shifts towards the tensile side. However, for computational simplicity, for now, we can assume that the neutral axis remains at the center of the specimen throughout the bending process, and the strain can be calculated as follows:

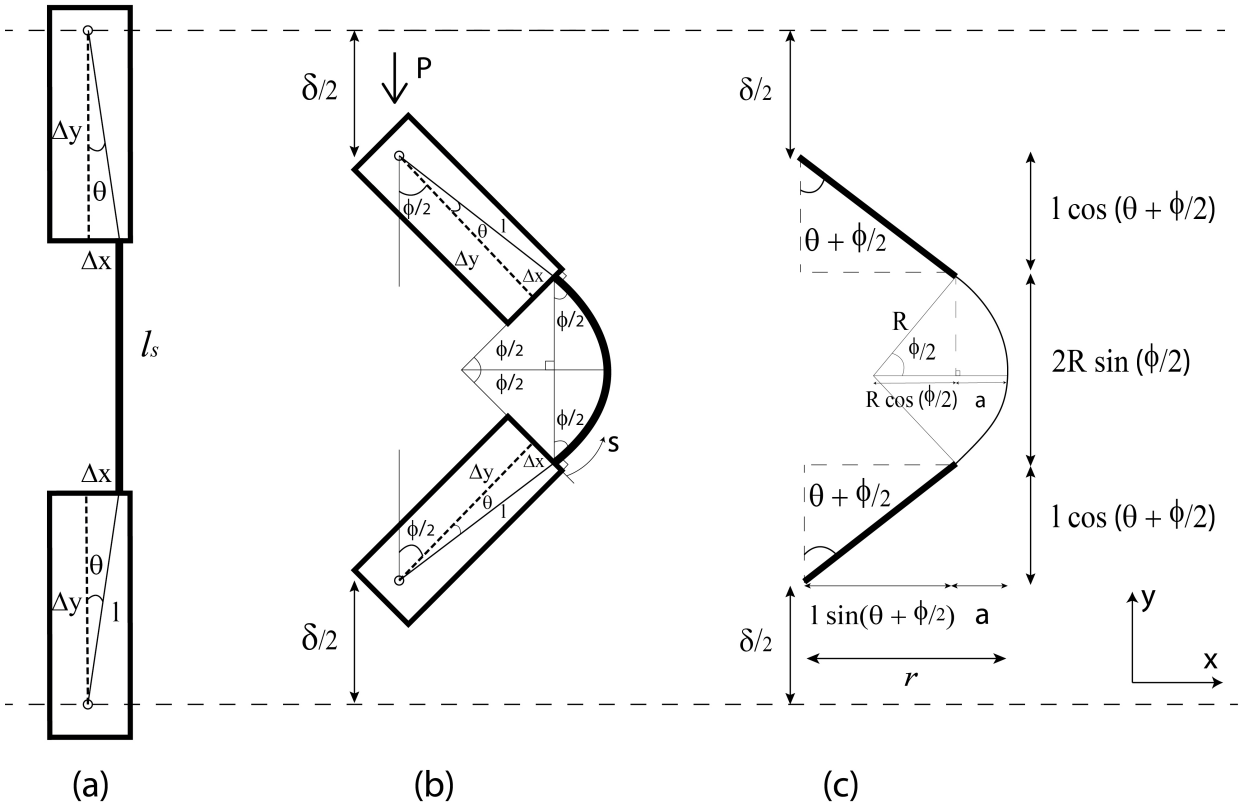


**Fig. 2 Geometry of the Column Bending Test : (a) Initial test geometry, (b) angles and (c) distances in the test setup when a displacement $\delta$ is applied [21].**

$$\varepsilon = \frac{\kappa t}{2}. \tag{4}$$

The maximum moment, which occurs at the center of the specimen, is given by:

$$M_{max} = Pr. \tag{5}$$

The minimum moment, which occurs at the coupon edges near the grips, is given by:

$$M_{min} = Pl\sin(\theta + \frac{\phi}{2}). \tag{6}$$

## III. Analysis of the Column Bending Test using elastica theory

The closed form solution assumes a constant curvature across the arclength. However, in reality, the curvature varies across the arclength, with the maximum curvature being obtained at the center of the bent specimen. In order to capture this effect of variation in curvature, the specimen needs to be modeled using Euler's theory of elastica. This large deformation theory accurately captures significantly varying curvatures occurring as a result of large scale deflection of stuctural elements.

Assuming the response to be linear, the constitutive relationship between moment and curvature is given by:

$$M(s) = EI\kappa(s) = EI\alpha'(s). \tag{7}$$

where $M(s)$ represents the varying bending moment across the arclength parameter $s$, $E$ represents the Young's modulus of the HSC specimen which is assumed to be constant throughout the test, $I$ represents the area moment of inertia of specimen, $\kappa(s)$ represents the varying curvature at every point along the arclength, and $\alpha$ represents the angle between a vector tangent to the coupon and the vertical axis at every point along the curve. The differential equations for the position co-ordinates $x(s)$ and $y(s)$ can be given in terms of the angle $\alpha(s)$ as:

$$\frac{dx}{ds} = \sin\alpha \,, \tag{8}$$

$$\frac{dy}{ds} = \cos\alpha \,. \tag{9}$$

The bending moment can be expressed as:

$$EI\frac{d\alpha}{ds} = M = P\left(x + l\sin(\frac{\phi}{2} + \theta)\right). \tag{10}$$

where $x$ is the horizontal distance to the loading axis, $P$ is the applied load, $\theta$ is the arm angle resulting from the initial offset distance $\Delta x$ and $\phi$ is twice the angle of each rigid arm with the vertical axis.

A numerical integration on Matlab was performed using the 'ode45' command. The boundary conditions considered were $\theta_{midpoint} = 0$, $x_0 = 0$ and $y_0 = 0$. Since it is not possible to integrate these equations without a given value for the applied load, a shooting algorithm was implemented. The algorithm was used to evaluate the applied loading necessary to satisfy the condition $\theta_{midpoint} = 0$. For a given load and the vertical displacement $\delta$ of the testing machine, the numerical integration solved for the shape of the specimen as well as captured the varying curvature across the arclength of the bent specimen.

## IV. Effect of various testing parameters involved in the Column Bending Test on failure properties of the laminate

In the sub-sections that follow, the dimensions of the rigid arms correspond to that of the typical arms used in-house, as well as at Roccor, with $\Delta x_{nom}$ and $\Delta y$ values equal to 0.3175 mm and 31.623 mm respectively. Moreover, we define a parameter, the normalized free length $\xi$, given by:

$$\xi = \frac{2l}{l_s} \quad . \tag{11}$$

which describes the ratio of the size of both the rigid arms w.r.t. the specimen free length. A large value of $\xi$ is representative of rigid arms that are relatively longer compared to the free length of the specimen.

### A. Effect of errors due to uncertainty of variation in free length

Various factors during the test may give rise to an uncertainty in the free length of the specimen. First, these variations might occur due to incorrect sample preparation. Next, changes in free length might occur during the test due to slippage between the coupon grips and the specimen owing to the large forces involved at the clamp ends. These factors ultimately affect the failure strain. Hence, it is essential to quantify the errors incurred due to variations in free length.

Figure 3 shows the percent error in curvature as a function of percent error in free length, for various free length values between 10 mm and 40 mm. These free length values were chosen based on the current set of tests being conducted in-house, and is typical of values commonly used for CBT. For a given free length, these plots have been evaluated for the same value of the test displacement for all cases involving errors in free length from $-10\%$ to $10\%$ . The value of this test displacement corresponds to a net rotated angle of 90 degrees for the nominal length case (which has no error in free length). The errors in curvature have been evaluated using both elastica and the closed form solution.

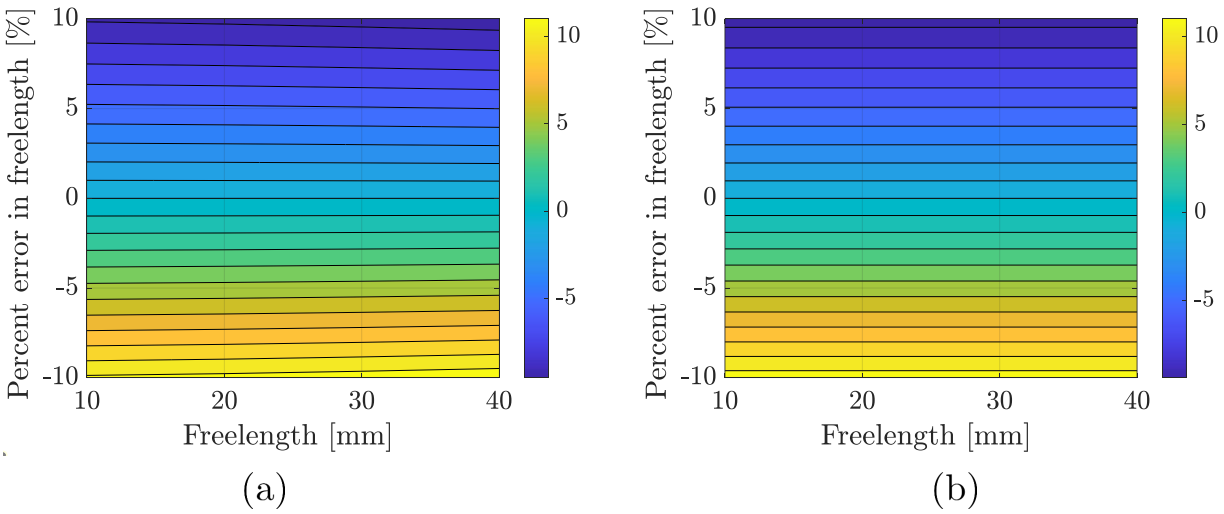


**Fig. 3 Percent error in curvature as a function of error in free length and free length obtained using: a) Elastica solution and b) Closed form solution.**

The plots show that both methods give nearly the same values for the error, with relatively minor differences. Further, we can observe that for a given percentage error in free length , the percentage error in curvature remains nearly constant, regardless of free length. The value of this percent error in curvature is nearly equal to the percent error in free length, with minor differences depending on whether the change in free length is positive or negative. If the free length errors are positive (i.e. true free length is larger than the measured free length), the numerical value for the percent error in curvature is slightly smaller than the numerical value for the percent error in free length. Conversely, if the free length errors are negative, the opposite is true. These plots can help give an estimate of the errors in curvature that we could expect for given errors in free length.

### B. Effect of errors in initial offset distance on curvature

The initial offset distance, referred to as $\Delta x$ in Figure 2, is an important parameter that determines the direction of bending during CBT. Its value depends on the manufacturing precision of the rigid arms as well as the specimen thickness, which is usually neglected in the calculations. Errors in manufacturing of the arms, or the specimen may induce errors in the value of the initial offset distance, and hence, it is essential to quantify its eventual implication on failure curvature.

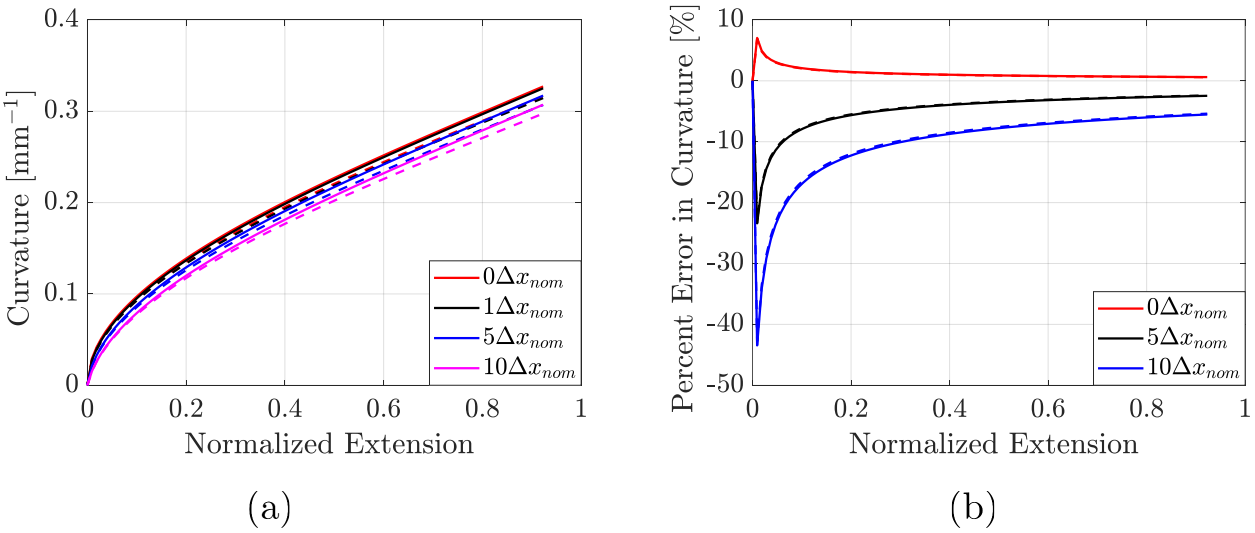


**Fig. 4 Effect of $\Delta x$ on curvature for a specimen having $l_s = 10$ mm. The solid lines represent the curvature values predicted by the elastica, whereas the dashed lines represent those predicted by the closed form solution. (a) Curvature as a function of normalized extension, and (b) percent error in curvature as a function of normalized extension for different values of $\Delta x_{nom}$.**

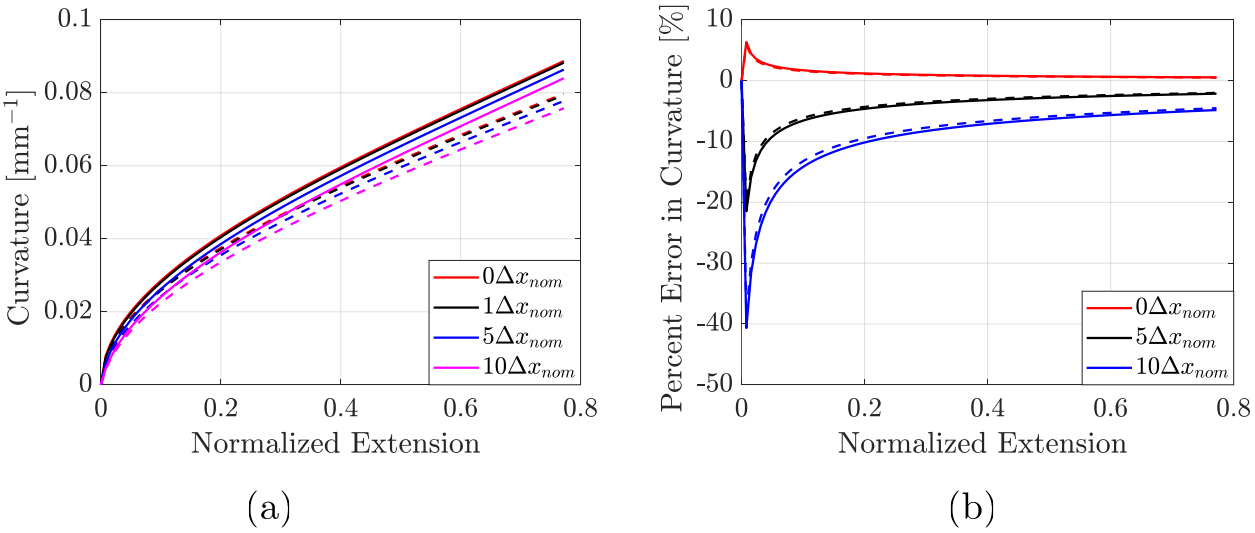


**Fig. 5 Effect of $\Delta x$ on curvature for a specimen of $l_s = 40$ mm. The solid lines represent the curvature values predicted by the elastica, whereas the dashed lines represent those predicted by the closed form solution. (a) Curvature as a function of normalized extension, and (b) percent error in curvature as a function of normalized extension for different values of $\Delta x_{nom}$.**

Figures 4 and 5 illustrate the effect of $\Delta x$ on curvature for specimens having free lengths 10 mm and 40 mm respectively. As mentioned in the previous section, these free lengths are typical of those utilized for CBT. The solid and the dashed lines correspond to the values predicted by the elastica and the closed form solution respectively. The x axis in these plots represents the normalized extension, where the normalization is done with respect to the total initial vertical distance corresponding to the case having no net rotation for the rigid arms and the coupon, as seen in Figure 2a. The values for percent error in curvature are evaluated with respect to the nominal case consisting of $\Delta x = \Delta x_{nom}$.

From Figures 4 and 5, we can also observe that the percent error in curvature is nearly the same regardless of the free length, following a similar trend for both plots. The error is higher at the beginning, and eventually flattens out to a

value less than 5% as the test proceeds. This indicates that the effect of $\Delta x$ on curvature becomes much lesser as the specimen bends more and more, which indicates that it is desirable to have the specimen fail at a much higher rotated angle of the rigid arms in order to minimize the error incurred due to incorrect evaluation of $\Delta x$.

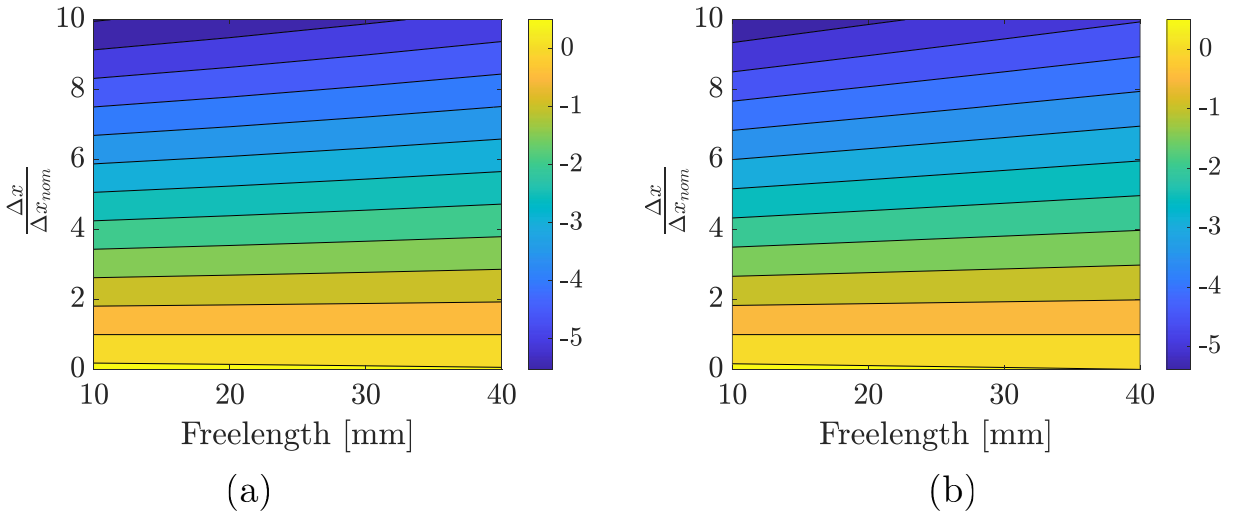


**Fig. 6 Percent error in curvature for different values of $\Delta x$ and free length obtained using: a) Elastica solution and b) Closed form solution.**

Figure 6 displays the effect of $\Delta x$ on curvature for different values of free length. For a given free length, these plots have been evaluated for the same value of test displacement for all $\Delta x$ values ranging from 0 to $10\Delta x_{nom}$. The value of this test displacement corresponds to a net rotated angle of 90 degrees for the nominal case, *i.e.* $\Delta x = \Delta x_{nom}$. The errors have been evaluated using both elastica and the closed form solution. As can be seen from the plots, the errors are within 6% even for an initial offset distance value of $10\Delta x_{nom}$ which is a significant variation of $\Delta x$. This indicates that $\Delta x$ does not play much of a role if the failure of the specimen takes place at a net rotated angle of 90 degrees for the rigid arms.

### C. Effect of pre-conditioning on failure strain of coupons

In this section, we explore the effect of subjecting the samples to an initial pre-determined strain before conducting the actual test of the specimens. This effect, also known as pre-conditioning, is expected to reduce the standard deviation in failure strain amongst different specimens subjected to the exact same loading conditions. Moreover, it is expected that pre-conditioning also helps mitigate the effects of manufacturing error. However, the effect of pre-conditioning on failure strain of thin CFRP laminates is still not understood. In order to further explore this phenomenon, an investigation was conducted to understand the effect of the number of cycles of pre-conditioning, as well as the magnitude of the pre-determined strain, and its eventual effect on the failure strain of the specimens. The selected laminated laminate for study was $GF_{PW}$-$IM7_{UD}$-$GF_{PW}$. Here, the $GF_{PW}$ indicates glass fiber plain weave, whereas $IM7_{UD}$ indicates unidirectional laminate of IM7 carbon fibers. The $GF_{PW}$ was 68 GSM per layer, whereas the $IM7_{UD}$ was 110 GSM per layer. The inner $IM7_{UD}$ was oriented along the loading direction, whereas the outer $GF_{PW}$ was oriented at 45° with respect to the inner $IM7_{UD}$ layer. The matrix used was PMT-F7, which was procured from Patz Materials and Technologies. For the fabrication, the laminates were first placed in layers according to their respective orientation, and then placed between two aluminum sheets. This assembly was then vacuum sealed together and placed in an oven until curing occured. The individual samples were then cut using a shear cutter. The nominal length of each coupon was 38.1 mm. The free length, width and thickness of each coupon was 7.62 mm, 25.4 mm and 0.38 mm respectively. Failure was defined as the point where the drop in moment was 1% w.r.t. the highest moment observed in the test. The strains were evaluated using the closed form solution since it has been shown previously [21] that for larger values of $\xi$ ($\xi = 8.3$ in this case), the curvature predictions are quite accurate and the errors are within 5%.

| Test | No preconditioning | | 2.99% (1.99 %) | | 3.02% (2.03 %)×5 | | 4.38% (2.94 %) | | 4.5% (3 %) ×5 | |
|---|---|---|---|---|---|---|---|---|---|---|
| | Surface | IM7 | Surface | IM7 | Surface | IM7 | Surface | IM7 | Surface | IM7 |
| S.1 | 4.93 | 3.12 | 5.38 | 3.56 | 4.54 | 2.93 | 5.09 | 3.23 | 5.82 | 3.97 |
| S.2 | 4.75 | 3.32 | 4.94 | 3.19 | 4.81 | 3.14 | 5.56 | 3.86 | 5.14 | 3.41 |
| S.3 | 4.43 | 2.96 | 5.12 | 3.23 | 4.68 | 3.15 | 4.63 | 3.06 | 5.06 | 3.22 |
| S.4 | 4.53 | 2.93 | 4.25 | 2.91 | 4.98 | 3.20 | 5.13 | 3.47 | 4.73 | 3.17 |
| S.5 | 5.21 | 3.35 | 5.20 | 3.54 | 4.50 | 3.05 | 5.11 | 3.27 | 4.96 | 3.18 |
| S.6 | 4.83 | 3.08 | 4.37 | 2.82 | 5.10 | 3.34 | 5.13 | 3.54 | 4.92 | 3.43 |
| S.7 | 4.30 | 3.00 | 5.81 | 4.14 | 5.44 | 3.67 | 4.74 | 3.21 | 5.27 | 3.68 |
| S.8 | 4.82 | 3.33 | 5.45 | 3.70 | 5.12 | 3.30 | 4.71 | 3.18 | 4.89 | 3.24 |
| S.9 | 5.10 | 3.40 | 4.93 | 3.22 | 4.38 | 2.93 | 5.45 | 3.78 | 5.49 | 3.86 |
| S.10 | 4.92 | 3.17 | 5.00 | 3.41 | 5.25 | 3.46 | 5.01 | 3.36 | 5.41 | 3.66 |
| S.11 | - | - | - | - | 5.06 | 3.30 | - | - | - | - |
| Mean | 4.78±0.29 | 3.17±0.17 | 5.05±0.47 | 3.37±0.39 | 4.89±0.34 | 3.22±0.23 | 5.17±0.33 | 3.39±0.26 | 5.17±0.33 | 3.48±0.29 |

**Table 1 Strain at failure (in percent) at the surface of both, the outer GF layer as well as the inner IM7 layer. The first column represents samples that did not experience any pre-conditioning. The second and fourth columns represent samples that experienced one cycle of preconditioning, whereas samples in the third and fifth columns experienced five cycles. The pre-determined strain values of approximately 3% and 4.5% on the GF surface, with a corresponding strain of 2% and 3% respectively on the IM7 surface, were obtained by subjecting the samples to a prescribed test displacement of 0.5 inch and 1 inch respectively.**

The results are shown in Table 1. For evaluating the strain, the neutral axis was assumed to be at the center of the coupon throughout the test. These strains were evaluated separately for the outer surface of the coupon (i.e. the GF layer), and the surface of the IM7 layer. Samples were divided into five groups. The first set of samples did not experience any pre-conditioning. These are represented in the first column of Table 1. For the samples that experienced pre-conditioning, the pre-determined strains were chosen such that a strain of approximately 3% and 4.5% respectively was obtained on the GF surface, and 2% and 3% respectively was obtained on the IM7 surface. These strain values were obtained by subjecting the samples to a prescribed pre-conditioning displacement of 0.5 inch and 1 inch respectively.

In Table 1, the second and fourth columns represent samples that experienced one cycle of preconditioning. These occurred at a strain of 2.99% and 4.38% respectively at the GF surface, with a corresponding strain of 1.99% and 2.94% respectively at the IM7 surface. The third and fifth columns represent samples that were subjected to five cycles of pre-conditioning. These occurred at a strain of 3.02% and 4.5% respectively at the GF surface, with a corresponding strain of 2.03% and 3% respectively at the IM7 surface. About ten samples were tested for each case and the corresponding strain at failure (in percent) has been listed in Table 1 at the surface of both, the outer GF layer as well as the inner IM7 layer. As seen from the data, no clear correlation was found between samples that experienced preconditioning and those that did not.

## V. Correction factor to improve the accuracy of moment-curvature predictions

The closed form solution that is used to obtain the moment-curvature response of specimens subjected to CBT assumes that the moment and the curvature are constant across the arclength of the bent specimen. In other words, the bent specimen is modeled as a circle of varying radius throughout the test. However, it has been shown previously [21] that this assumption can result in errors in the moment-curvature response. This section provides a correction factor to account for errors incurred when assuming constant curvature. The correction factors will be defined as the ratio between the geometrically-exact results obtained through the elastica, and those assuming a circle:

$$\zeta_\kappa\left(\xi, \frac{\delta}{L}\right) = \frac{\kappa_{max,el}}{\kappa_{max,g}} \quad , \tag{12}$$

$$\zeta_D\left(\xi, \frac{\delta}{L}\right) = \frac{\left(\frac{\partial M}{\partial \kappa}\right)_{el}}{\left(\frac{\partial M}{\partial \kappa}\right)_{g}} \quad . \tag{13}$$

where $\zeta_\kappa$ and $\zeta_D$ represent the correction factors for curvature and the bending stiffness respectively, and $\kappa_{max,el}$ and $\kappa_{max,g}$ are the maximum curvature predicted by the elastica and the closed form geometric solution, respectively. Additionally, $\left(\frac{\partial M}{\partial \kappa}\right)_{el}$ and $\left(\frac{\partial M}{\partial \kappa}\right)_{g}$ represent the bending stiffness predicted by the elastica and the geometric closed form solution respectively. The correction factors $\zeta_\kappa$ and $\zeta_D$ are dependent on the parameters $\xi$ and $\delta/L$. This is due to the fact that these correction factors are derived from the errors in curvature and bending stiffness which are themselves functions of $\xi$ and $\delta/L$.

In order to obtain both the correction factors, a fitting was done individually for each of these functions. Typically, testing using CBT involves $\xi$ values between 1 and 4. In order to obtain an accurate fit, five hundred equally spaced $\xi$ values were chosen between 0.5 and 8, and correction factors were obtained for each of these using Equations 12 and 13 for the case involving no softening.

A parabolic fit was used to capture the variation of the correction factor as a function of $\frac{\delta}{L}$ for each $\xi$. The coefficients of these parabolae were recorded, so as to identify the function that accurately captures the values of these coefficients as a function of $\xi$. An analytical function for each of the correction factors was then obtained. The MATLAB curve fitting tool was used for this purpose. The correction factor function for curvature can be given by:

$$\zeta_\kappa\left(\xi, \frac{\delta}{L}\right) = a(\xi)\left(\frac{\delta}{L}\right)^2 + b(\xi)\left(\frac{\delta}{L}\right) + c(\xi) \quad . \tag{14}$$

$$a(\xi) = 0.04(\xi^{-0.45}) - 0.01 \quad . \tag{15}$$

$$b(\xi) = 0.03(\xi^{-0.6}) - 0.005 \quad . \tag{16}$$

$$c(\xi) = 0.13(\xi^{-0.6}) + 1 \quad . \tag{17}$$

The correction factor function for bending stiffness can be given by:

$$\zeta_D\left(\xi, \frac{\delta}{L}\right) = a(\xi)\left(\frac{\delta}{L}\right)^2 + b(\xi)\left(\frac{\delta}{L}\right) + c(\xi) \quad . \tag{18}$$

$$a(\xi) = \frac{0.15\xi - 0.125}{\xi^2 - 0.35\xi + 0.3} \quad . \tag{19}$$

$$b(\xi) = 0.1(\xi^{-0.8}) - 0.01 \quad . \tag{20}$$

$$c(\xi) = 0.13(\xi^{-0.6}) + 1 \quad . \tag{21}$$

The error between the the correction factor, obtained using analytical equations 14 and 18, and the actual computed values for the correction factor is shown in Figure 7. The error between the analytical equations and the computed values are within 2 %, thereby indicating the validity of the correction factor analytical function for the desired range of $\xi$ values between 0.5 and 8. For comparison, the errors are around 20 % without the correction factor for $\xi = 0.5$, as observed in a previous work [21].

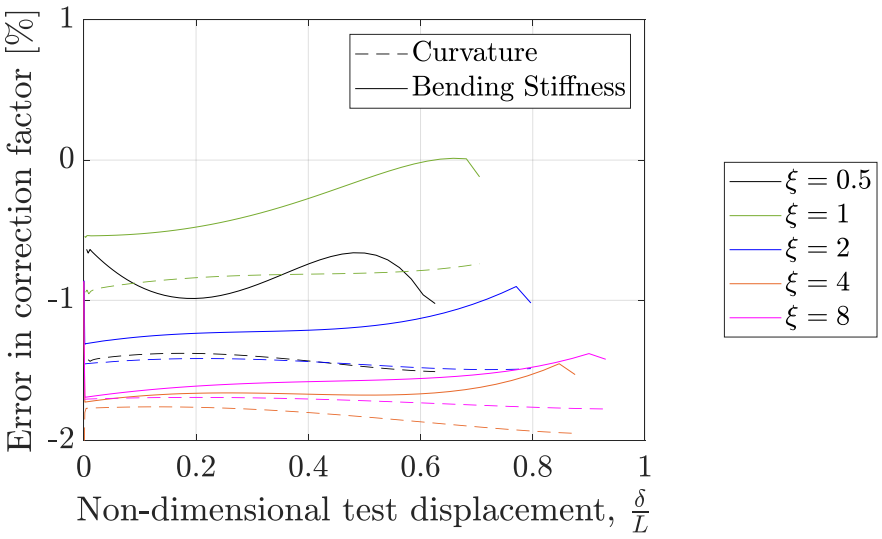


**Fig. 7 Comparing the error in the correction factor for curvature and bending stiffness, obtained using analytical equations 12 and 18, and the actual values for the correction factor obtained from a previous work [21].**

## VI. Conclusion

In this paper, we have analyzed the effect of various testing parameters involved in the Column Bending Test (CBT) on the failure properties of HSCs. CBT is the currently preferred method to obtain the moment-curvature response of HSCs. It combines the best possible features of the platen test and the Large Deformation Four Point Bending Test (LDFPB), the traditionally utilized testing methods that were previously used to obtain the failure properties of HSCs. In particular, we studied the effect of three different phenomenon incurred during testing of HSCs and their implications on the failure strain: (1) error in free length of the coupon, (2) error in initial offset distance of the rigid arms, and (3) effect of subjecting samples to an initial pre-determined strain (also known as pre-conditioning). Further, we also established an improved formula to evaluate the curvature and bending stiffness using CBT.

In order to determine the error that occurs due to uncertainty in the variation of free length, we varied the free length between 10 mm and 40 mm, which are typical of the free length values used for CBT. The error in free length was chosen to be between -10 % and 10 %. For a particular value of free length, error in curvature was obtained for the same value of test displacement for all cases of errors in free length for that particular free length. This value of this test displacement was chosen based on a net rotated angle of 90° for the rigid arms, for the nominal case where the free length is assumed to have no error. Results were obtained using both Euler's elastica, which models large scale deformation of 1D structural elements, and the closed form solution, which is obtained using a simplified geometric analysis of CBT by assuming the bent specimen as a circle. We found that both methods resulted in nearly the same value of the error for the curvature. Also, the percentage error in curvature was nearly constant for a given percent error in free length and approximately equal to this percent error in free length value, regardless of the free length value.

Next, we also studied the effect of error in the initial offset distance. This initial offset distance is a design parameter provided during manufacturing of the rigid arms, and has a different value based on the design of the arms. This initial offset distance helps ensure that the specimen bends in the desired direction when the test starts. We found that the error in curvature due to error in the initial offset distance eventually flattens out to a value less than 5 % as the test displacement increases, and that it is desirable to have the specimen fail at a higher net rotated angle of the rigid arms to ensure that the error in curvature is minimized due to an incorrect initial offset distance. Moreover, for a net rotated angle of 90° for the rigid arms, the error in curvature is within 6 % even for a huge value of initial offset distance of $10\Delta x_{nom}$.

Subjecting samples to an initial pre-determined strain has been suggested as a method to reduce variation in failure strain between different samples. The effect of this preconditioning on the failure strain of HSCs was investigated as a

part of this study. The laminate considered for the study was $GF_{PW}$-$IM7_{UD}$-$GF_{PW}$, where the $IM7_{UD}$ was aligned with the loading direction. The pre-determined strains were chosen such that a strain of approximately 3% and 4.5 % respectively was obtained on the GF surface, and 2 % and 3 % respectively was obtained on the IM7 surface. The number of cycles of pre-conditioning was also varied and set to either one or five cycles. Overall, no correlation was found between samples that experienced preconditioning and those that did not, and that the degree of preconditioning may not have a significant effect on failure strain of specimens.

A previous study by the authors [21] demonstrated the errors that occur as a result of the constant curvature assumption in determining the bending response of laminates subjected to CBT. In this work, we propose an improved formula to determine the curvature and bending stiffness. The new formula gives an error of less than 2 % even for relatively smaller grip to freelength ratios ($\xi = 0.5$ in this case) than the ones used in actual practice. For comparison, the error is around 20% without the incorporation of the correction factor the $\xi = 0.5$ case. This improved formula will help the HSC community obtain better predictions for the bending response of HSCs tested using CBT.



## Acknowledgments

Funding from Roccor LLC, through the Air Force STTR Program, contract FA9453-17-P-0463, is gratefully acknowledged.

## References

[1] McEachen, M., "Validation of SAILMAST Technology and Modeling by Ground Testing of a Full-Scale Flight Article," *48th AIAA Aerospace Sciences Meeting Including the New Horizons Forum and Aerospace Exposition*, 2010, p. 1491.

[2] Mobrem, M., and Adams, D., "Lenticular jointed antenna deployment anomaly and resolution onboard the Mars Express spacecraft," *Journal of Spacecraft and Rockets*, Vol. 46, No. 2, 2009, pp. 403–410.

[3] Baier, H., Datashvili, L., Nathrath, N., and Pellegrino, S., "Technical assessment of high accuracy large space borne reflector antenna," *Final report of ESA contract*, , No. 16757/02, 2004.

[4] Soykasap, O., Pellegrino, S., Howard, P., and Notter, M., "Folding large antenna tape spring," *Journal of Spacecraft and Rockets*, Vol. 45, No. 3, 2008, pp. 560–567.

[5] Pollard, E., and Murphey, T., "Development of deployable elastic composite shape memory alloy reinforced (DECSMAR) structures," *47th AIAA/ASME/ASCE/AHS/ASC Structures, Structural Dynamics, and Materials Conference 14th AIAA/ASME/AHS Adaptive Structures Conference 7th*, 2006, p. 1681.

[6] Spence, B. R., and White, S. F., "Directionally controlled elastically deployable roll-out solar array," , Apr. 1 2014. US Patent 8,683,755.

[7] Yee, J., and Pellegrino, S., "Biaxial bending failure locus for woven-thin-ply carbon fibre reinforced plastic structures," *46th AIAA/ASME/ASCE/AHS/ASC Structures, Structural Dynamics and Materials Conference*, 2005, p. 1811.

[8] Sanford, G. E., Ardelean, E. V., Murphey, T. W., and Grigoriev, M. M., "High Strain Test Method for Thin Composite Laminates," *16th International Conference on Composite Structures. Porto, Portugal*, 2011.

[9] Fernandez, J. M., and Murphey, T. W., "A Simple Test Method for Large Deformation Bending of Thin High Strain Composite Flexures," *2018 AIAA Spacecraft Structures Conference*, 2018, p. 0942.

[10] Herrmann, K. M., *An Investigation of a Vertical Test Method for Large Deformation Bending of High Strain Composite Laminates*, 2017.

[11] López Jiménez, F., and Pellegrino, S., "Folding of fiber composites with a hyperelastic matrix," *International Journal of Solids and Structures*, Vol. 49, No. 3-4, 2012, pp. 395–407.

[12] Rose, T., Sharma, A., Seamone, A., López Jiménez, F., and Murphey, T., "Carbon Unidirectional Composite Flexure Strength Dependence on Laminate Thickness," *Proceedings of the American Society for Composites—Thirty-third Technical Conference*, 2018.

[13] Medina, K., Rose, T., and Murphey, T. W., "Initial Investigation of Time Dependency on Failure Curvatures of FlexLam High Strain Composites," *Proceedings of the American Society for Composites—Thirty-second Technical Conference*, 2017.

[14] Medina, K., Rose, T., and Francis, W., "Long-term Stress Rupture Limitations of Unidirectionasl High Strain Composites in Bending," *Proceedings of the American Society for Composites—Thirty-third Technical Conference*, 2018.

[15] Rose, T., Medina, K., Francis, W., Kawai, K., and Fernandez, J., "Viscoelastic Behaviors of High Strain Composites," *2019 AIAA Spacecraft Structures Conference*, 2019.

[16] Schlothauer, A., Pappas, G. A., and Ermanni, P., "Material response and failure of highly deformable carbon fiber composite shells," *Composites Science and Technology*, Vol. 199, 2020, p. 108378.

[17] Adamcik, B., Firth, J., Pankow, M., and Fernandez, J. M., "Impact of Storage Time and Operational Temperature on Deployable Composite Booms," *AIAA Scitech 2020 Forum*, 2020, p. 1183.

[18] Kang, J. H., Hinkley, J. A., Gordon, K. L., Thibeault, S. A., Bryant, R. G., Fernandez, J. M., Wilkie, W. K., Morales, H. E. D., Mcgruder, D. E., Peterson, R. S., et al., "Viscoelastic characterization of polymers for deployable composite booms," *Advances in Space Research*, 2020.

[19] Gomez-Delrio, A., "Viscoelastic Analysis of High Strain Composites for Deployable Structures in Space Applications," 2020.

[20] Zehnder, A., Patel, V., and Rose, T., "Micro-CT Imaging of Fibers in Composite Laminates under High Strain Bending," *Experimental Techniques*, Vol. 44, No. 5, 2020, pp. 531–540.

[21] Sharma, A. H., Rose, T., Seamone, A., Murphey, T. W., and López Jiménez, F., "Analysis of the Column Bending Test for Large Curvature Bending of High Strain Composites," *AIAA Scitech 2019 Forum*, 2019, p. 1746.